ADVANCES IN FOREST FIRE RESEARCH

2022

Edited by
DOMINGOS XAVIER VIEGAS
LUÍS MÁRIO RIBEIRO

Flame spread and combustion dynamics in pine litter under unsteady wind conditions

Eric V Mueller*[1]; Zakary Campbell-Lochrie[2]; Carlos Walker-Ravena[2]; Matt Patterson[3]; Jason Cole[3]; Michael R Gallagher[3]; Kenneth L Clark[3]; Nicholas S Skowronski[3]; Rory M Hadden[2]

[1] National Institute of Standards and Technology. Gaithersburg, MD, USA, {eric.mueller@nist.gov}
[2] University of Edinburgh. Edinburgh, UK, {Z.Campbell.Lochrie, c.walkerravena, r.hadden@ed.ac.uk}
[3] USDA Forest Service Northern Research Station. Morgantown WV, Syracuse NY, and New Lisbon NJ, USA, {matthew.m.patterson, jason.cole2, michael.r.gallagher, kenneth.clark, nicholas.s.skowronski}@usda.gov

**Corresponding author*

Keywords

Flame spread, combustion dynamics, prescribed fire, field experiment, pine litter

Abstract

Understanding flame spread and combustion dynamics in surface fuels is important for both planning and evaluating the impact of prescribed fires. However, prescribed fires tend to be conducted under light and unsteady wind conditions as compared with those which have been well studied for wildfire scenarios. To improve this understanding and provide data for next-generation fire models, it is necessary to collect detailed time-resolved observations of these processes. To accomplish this, a series of small-scale field experiments was conducted in pine needle litter. 10 m x 10 m plots were constructed with fuel loads of either 0.5 kg/m2, 1.0 kg/m2, or 1.5 kg/m2. Wind was measured with an array of 17 anemometers and flame spread and combustion mode were monitored with an overhead infrared camera and thermocouple arrays. The light and gusty wind conditions resulted in unsteady fire behavior and a single relationship between wind speed and spread rate is unable to capture the range of behavior observed. A novel technique is introduced for identifying regions of flaming versus smoldering combustion in the infrared imagery. This approach indicates that flaming and smoldering times can be related directly to fuel loads, rather than wind conditions, though more work is required to link these times to burning rates. The implication is that dynamic flame spread in these conditions is difficult to predict without models that account for fire-atmosphere interactions. However, fuel consumption, and therefore prescribed fire effects, may be more straightforward to predict. This work has also resulted in a uniquely detailed dataset for testing fire models.

1. Introduction

Understanding and predicting fire behavior in relatively light and unsteady wind conditions is important in the context of prescribed fire. A quantitative approach to both planning these activities and evaluating their effectiveness relies on such an understanding (Hiers et al., 2020). For example, modelling the spread rate of fires can help practitioners plan specific burns to optimize desired objectives. However, unlike fires under strong wind conditions (typical of wildfires) and steady or zero wind conditions (typical of laboratory studies), realistic burning conditions during prescribed fires often involve light, dynamic winds where fire-induced buoyant flows may become dominant. In order to investigate the effect of these conditions, and to provide detailed data for modeling efforts, a series of field experiments was conducted in pine needle litter. The aim of this work is to analyze highly-resolved measurements of flame spread and combustion to determine the relative roles of fuel structure and wind at fine scale, under conditions relevant to prescribed burning.

2. Methods

Experiments were carried out on a 10 m x 10 m plot (see Figure 1) within a pitch pine/loblolly pine plantation in the Pinelands National Reserve of New Jersey. A total of 35 experiments were conducted under various fuel and weather conditions; however, this analysis focuses on a subset of 19 of these for which fire spread

successfully across the plot and the measurements made were consistent. The fuel beds consisted of pitch pine (*Pinus rigida* Mill.) needles or an equal mix of pitch pine needles and oak (predominantly *Quercus montana Willd.*) leaves from local sources. The beds were manufactured to achieve average loadings of nominally 0.5 kg/m^2, 1.0 kg/m^2, or 1.5 kg/m^2, in order to represent different prescribed fire return intervals. Burns were carried out in ambient temperatures between 17 °C and 31 °C, relative humidity between 22 % and 66 %, and fuel moisture contents between 5.9 % and 14.4 %.

2.1. Wind measurement

Wind was measured with an array of 17 3D sonic anemometers (Figure 1). One of these was located at the plot center at a height of 10 m Above Ground Level (AGL), while the remaining 16 were in a 4x4 grid at nominally 3.0 m AGL. All anemometers were sampled at a frequency of 10 Hz.

For this analysis, a characteristic time-dependent horizontal wind vector was determined for each experiment. All anemometers were used for this calculation, to give an indication of the average wind across the experimental area. Previous measurements of ambient wind in the plantation indicated low sensitivity to height between the 2.5 m and 10 m levels (both are in the open sub-canopy space). Measurements of *u* and *v* velocity components were averaged independently, using 10-second moving average. Readings where the anemometer recorded a temperature in excess of 50 °C were rejected from this process, as they were within the fire plume and outside the operating range of the anemometer.

The spatial averaging procedure removes any localized features of the wind field, over the plot area, but allows for the fact that at any given moment, individual sensors may be impacted by the fire and not produce reliable data. The temporal averaging procedure removes some high frequency components of the signal in order to focus on the dominant behavior. The choice of a 10-second window was guided by the fact that mean winds were on the order of 1 m/s and the plot length was 10 m.

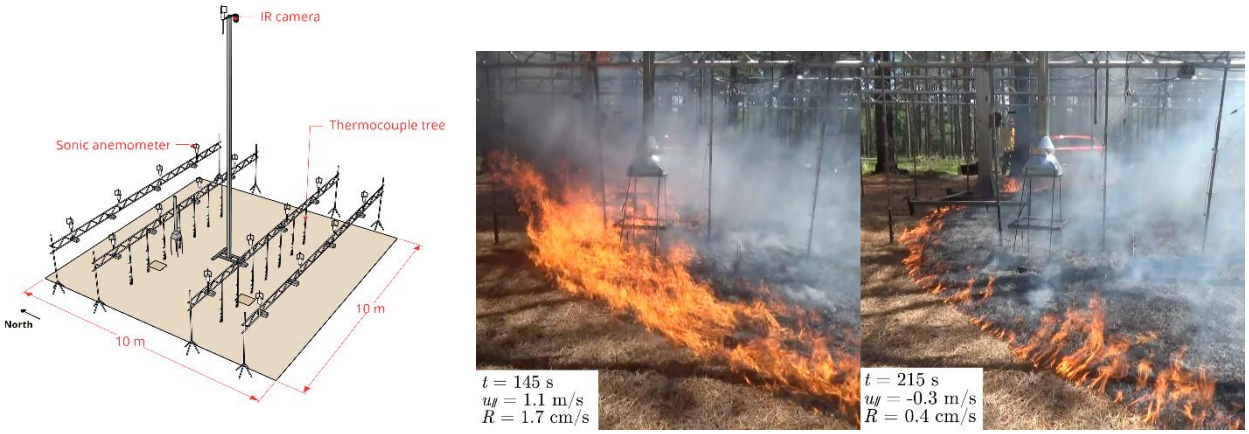

Figure 1- (left) Schematic of experimental plots; (right) example of fire spread during heading and backing conditions in a single experiment.

2.2. Flame spread

Infrared (IR) images were captured from a downward-facing IR camera placed at the center of the plot (Figure 1). The camera had a frame rate of nominally 25 Hz and provided a resolution of ~5 cm^2/pixel. True temperature measurement of the fuel bed is complicated by several factors (including unknown emissivity and possible emission and absorption by combustion products). However, the data are still valuable in a comparative sense, as described below, and temperatures are referred to as 'pixel' temperature rather than solid or gas phase.

The IR data were used to determine the progression of the leading edge of the flame front as a function of time. For each pixel, the arrival time of the flame front was determined by the corresponding temperature first exceeding 200 °C for a continuous period at least 1 second. The exact location of the flame front is sensitive to these criteria, but the advancement of the front is much less so.

Masks were applied to remove regions of spurious data where objects (e.g., camera support tower, instrumentation trusses, trees) obscure the view of the camera. Images were post processed and projected onto a Cartesian coordinate system. The spread rate, *R*, was calculated by taking the inverse of the gradient of the

arrival time matrix using and applying filtering and spatial averaging techniques to create a continuous spread map over the entire plot area (including masked regions).

Spread vectors with relevant corresponding arrival times were averaged to create a plot-average magnitude and direction of spread, excluding 1 meter of data on either flanking edge of the fire (dependent on the ignition edge). This approach allows the wind to be decomposed into the component in the direction of spread at a given moment, $u_{/\!/}$, and the component perpendicular, $u_{\perp}$, and the influence of wind could be analyzed independent of the compass direction at a given moment.

2.3. Combustion mode

An assessment of the combustion dynamics was conducted by estimating the duration of flaming and smoldering combustion for a given experiment. Separating these different combustion modes can prove quite difficult, particularly in the field. Visual assessment can be complicated by the obscuring presence of smoke and by the fact that the occurrence of smoldering combustion can be difficult to observe.

The IR imagery offers a solution to both problems; however, there is still a challenge in identifying the different regimes in the temperature signal for a given pixel. Both flaming and smoldering combustion may be associated with high temperatures in overlapping ranges, so it is not enough to simply apply thresholds. Further, the long-wave spectral range of the IR camera used here is poorly suited to observing emission from the flames.

Despite these challenges, visual inspection of the IR imagery shows that some presence of the flaming region can be detected. Because the flaming combustion zone is strongly affected by turbulence, we hypothesize that the ability to observe this region in the IR footage is a function of the rapid fluctuation in the temperature signal, rather than its absolute value. Therefore, we classified the combustion modes by analyzing these fluctuations.

A short-time Fast Fourier Transform was computed on the pixel noise, taken as the difference between the 25 Hz signal and a 1 Hz moving average. The average power at high frequency (> 4 Hz) was then computed. The maximum power was identified for each pixel, and the point at which the transient power falls below 5% of this value was taken as the threshold between flaming and smoldering. The onset of flaming was taken as the first point the 1-second moving average of temperature exceeds 200 °C, and the end of smoldering was taken as the final point above 200 °C. The resulting image of combustion times was then subjected to the same projection and spatial averaging as the spread rate map. This approach relies on user-selected thresholds for both the magnitude of the temperature and the magnitude of the signal noise. However, the calculation of flaming time was consistent with measurements made with thermocouples positioned at the top of the fuel bed (see Figure 1).

3. Results and discussion

3.1. Flame spread

Mean wind speeds were in the range of 0.5 m/s to 1.5 m/s, with relative standard deviations between 0.17 and 0.61. This gives an indication of the light and unsteady conditions; however, it does not account for shifts in wind direction which contribute to the dynamic fire behavior. Mean spread rates were in the range of 0.2 cm/s to 5.0 cm/s, with relative standard deviations between 0.26 and 1.73. To demonstrate the dynamic nature of individual burns, an example of the flame spread and wind calculation is shown in Figure 2. When the spread vector and the horizontal wind are not aligned there is necessarily a reduction in the magnitude of wind speed in the direction of spread ($u_{/\!/} \leq U$). An evaluation of the correlation between mean wind and spread, using Spearman's rank coefficient, yields a value of 0.22 (probability, p = 0.37) when using overall magnitude (U) and 0.53 (p = 0.02) when using magnitude in the direction of spread ($u_{/\!/}$). This points to the importance of capturing the dynamic wind in gusty conditions, rather than an average horizontal magnitude.

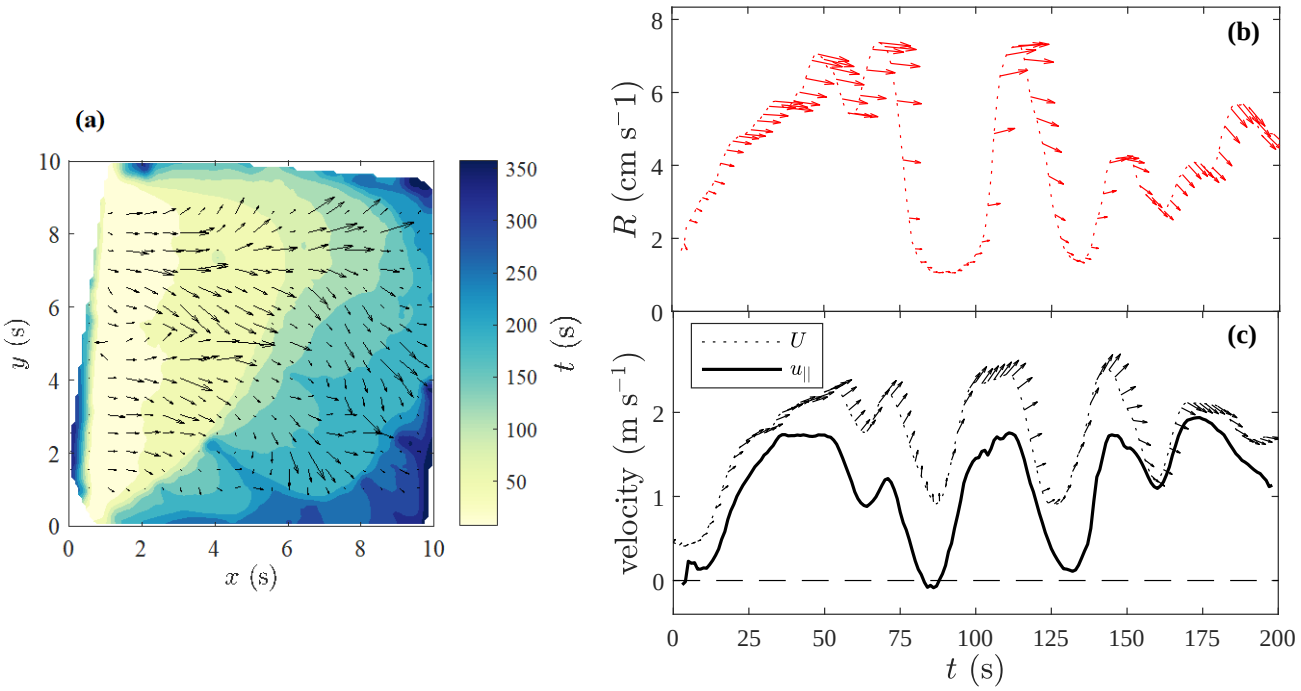

Figure 2- Example of fire spread analysis for one burn, ignited from the west (x = 0 m) with a fuel load of 0.5 kg/m². (a) The computed vectors of spread rate, overlaid on a contour plot of arrival time. (b) The time history of plot-average spread vectors. (c) The average wind vectors with the total magnitude (U), and wind magnitude in the direction of average spread ($u_{\parallel}$).

The analysis of spread rate and wind speed for all burns indicates a large scatter which cannot be accounted for with other environmental variables (fuel load, fuel moisture, relative humidity, ambient temperature). This is demonstrated by normalizing the spread by its value with no-wind, as shown in Figure 3. Large deviations occur when fitting to possible simple models for wind speed dependence. In fact, a hysteresis was observed in temporally resolved relationships of spread rate and wind. An assessment of Byram's convective number (Nelson, 1993) indicates the significant feedback between wind speed and spread rate is linked to the marginal conditions – fires are neither consistently plume dominated nor wind driven.

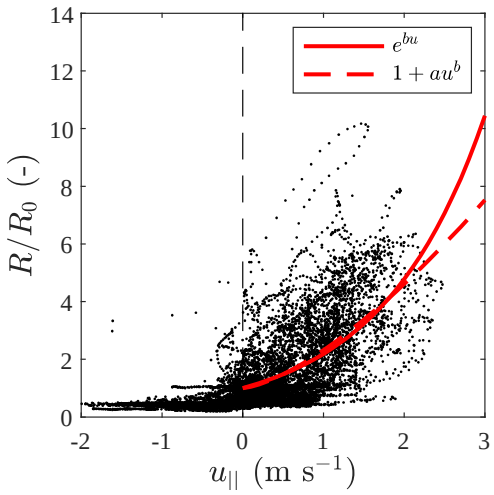

Figure 3- Relationship between instantaneous wind and spread rate. Spread rate is normalized against the average no-wind ($|u_{\parallel}|$<0.2 m/s) value for a given burn. Red lines are fits to common functions (Sullivan, 2009).

3.2. Combustion mode

An example of the analysis of flaming versus smoldering time is shown in Figure 4. The thermocouple and IR pixel temperature increase dramatically at the same time, indicating arrival of the fire front. Both maintain an elevated temperature for roughly 40 s, at which point the thermocouple temperature drops rapidly while the pixel temperature remains elevated. The power in the high-frequency noise in pixel temperature drops dramatically at the same time the flaming period ends, thus all remaining time at elevated temperature can be classified as smoldering.

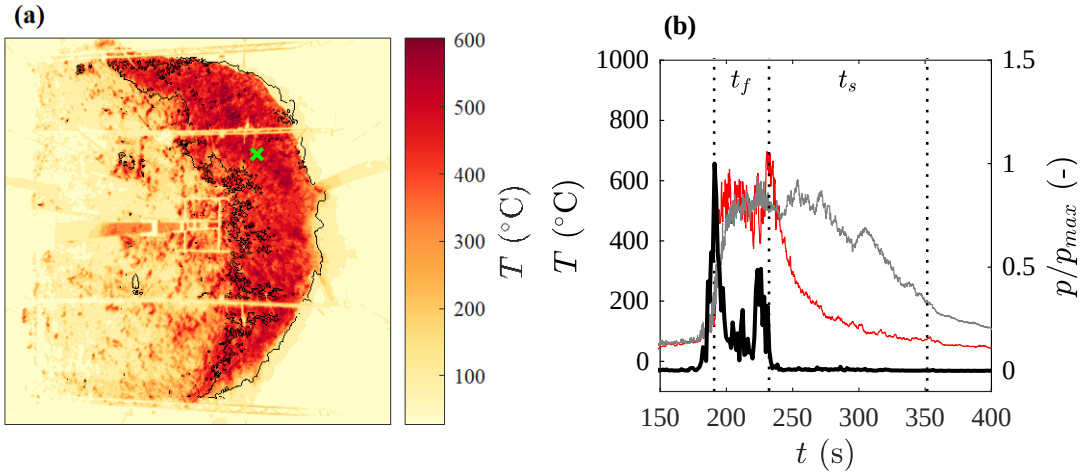

Figure 4- Example of fire spread analysis for one burn, ignited from the west (x = 0 m) with a fuel load of 1.5 kg/m^2. (a) Single frame of IR footage with sample point at the base of a thermocouple array shown as a green x. The region of active flaming is shown by the black contour line. (b) Time history at the sample point in (a): thermocouple temperature (red), pixel temperature (grey), and normalized power of noise (black). Duration of flaming (t_f) and smoldering (t_s) are shown by vertical lines.

The mean and standard deviations of both flaming and smoldering time are shown for each relevant burn in Figure 5. The duration of both combustion modes increases with fuel load, but the ratio may not be constant and requires more analysis. Preliminary results also indicate that wind speed is a less significant factor than fuel load under these conditions.

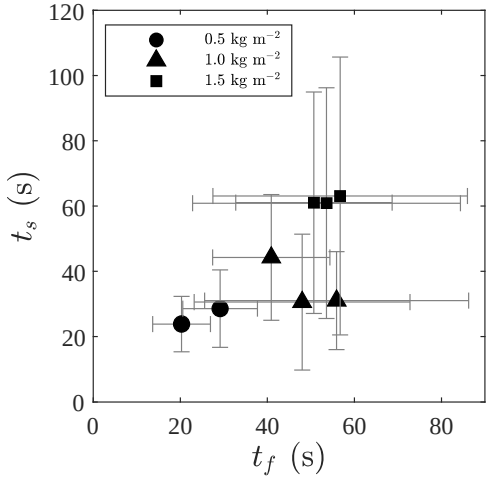

Figure 5- Average flaming time (t_f) and smoldering time (t_s) for all relevant pixels in each of the 8 burns. Error bars represent one standard deviation.

4. Conclusions

We observed a dynamic relationship between flame spread and ambient wind in conditions typical of prescribed burns. This is not fully captured by simple relationships which do not consider fire-atmosphere feedback. The experimental data can help to provide uncertainty bounds to these simple relationships. They can also act as test cases for more complex models which attempt to resolve such interactions and therefore require data with greater spatial and temporal resolution than is often available.

The combustion analysis provides a novel method for obtaining maps of flaming and smoldering times, though there are some limitations associated with this approach. The time of transition between flaming and smoldering can be evaluated against thermocouple data, but sensitivity to the noise threshold requires further examination. The optimal criteria to identify the end of smoldering using these diagnostics is also unknown. Further analysis may be able to identify combustion behavior specific to certain periods of fire behavior (e.g., heading or backing fire) or as a function of spatial fuel distribution. The inclusion of detailed fuel consumption information could also aid in estimating mass loss rates. The current analysis also has implications for understanding emissions and smoke plume development, as a function of the mode and distribution of energy release. Here again, there is also significant value for testing models of fire-atmosphere interactions. Such models either require a parameterization of energy release or endeavor to resolve it directly, but in either case a better understanding of combustion in field conditions is essential.

5. References

Hiers, J. K., O'Brien, J. J., Varner, J. M., Butler, B. W., Dickinson, M., Furman, J., Gallagher, M., Godwin, D., Goodrick, S. L., Hood, S. M., Hudak, A., Kobziar, L. N., Linn, R., Loudermilk, E. L., McCaffrey, S., Robertson, K., Rowell, E. M., Skowronski, N., Watts, A. C., & Yedinak, K. M. (2020). Prescribed fire science: the case for a refined research agenda. Fire Ecology, 16(1). DOI: 10.1186/s42408-020-0070-8

Nelson Jr, R. M. (1993). Byram derivation of the energy criterion for forest and wildland fires. International Journal of Wildland Fire, 3(3), 131–138. DOI: 10.1071/WF9930131

Sullivan, A. L. (2009). Wildland surface fire spread modelling, 1990–2007. 2: Empirical and quasi-empirical models. International Journal of Wildland Fire, 18(4), 369–386. DOI: 10.1071/WF06144